Development of a first-principles hybrid model for large-scale reheating furnaces[1]

Yukun Hu [a*], CK Tan [a], Jonathan Broughton [b], Paul Alun Roach [a]

[a] Faculty of Computing, Engineering and Science, University of South Wales, Pontypridd, CF37 1DL, United Kingdom

[b] Tata Steel R&D Swinden Technology Centre, South Yorkshire, S60 3AR, United Kingdom

Abstract

This paper details the development of a first-principles hybrid model capable of simulating transient thermal performances of a large scale reheating furnace. In particular, the new modelling approach combines the advantages of the classical zone method of radiation analysis and Computational Fluid Dynamics (CFD) in a robust manner, and overcomes the difficulties of incorporating three-dimensional flow field within a zone method based model. The developed model has been validated with comprehensive experimental data collected during an instrumented bloom trial period that includes a long production delay. The results suggest that the model predictions were in good agreement with the actual measurements, and that the model was able to respond correctly with respect to the encountered production delay during the trial.

Nomenclature

Abbreviations

CFD	Computational Fluid Dynamics
MCRT	Monte Carlo based Ray Tracing
MT	Measured Temperatures
PDEs	Partial Differential heat conduction Equations
PID	Proportional–Integral–Derivative
PT	Predicted Temperatures
ST	Set-point Temperatures
TEAs	Total Exchange Areas
ZM	Zone Model

Symbols

a_i	correlation coefficients	-
$a_{g,n}$, $a_{s,n}$	weighting coefficient in mixed grey gas model	-
A_d	area of furnace door	m^2
A_i	area of the i-th surface zone	m^2
A_j	area of the j-th door occupied surface zone	m^2
$b_{i,n}$	correlation coefficients	-
C_p	specific heat at constant pressure	$J\,kg^{-1}\,K^{-1}$
e	error	°C
E_c	combustion efficiency	-

---

[1] Part of this paper (Figures 14, 16; Table 3) was presented at the 7th International Conference on Applied Energy (ICAE2015), March 28-31, 2015, Abu Dhabi, UAE (Original paper title: "Development of transient mathematical models for a large-scale reheating furnace using hybrid zone-CFD methods" and Paper No.: 699).

* Corresponding author. Current address: School of Engineering, University of Warwick, Coventry, CV4 7AL, United Kingdom. Tel.: +44(0)24765 22333. E-mail: y.hu.9@warwick.ac.uk (Y. Hu)

E_f	furnace efficiency	-
F_{max}	proportion of maximum firing rate	-
F_{min}	proportion of minimum firing rate	-
$\overline{G_IG_J}, \overline{G_IS_J}, \overline{S_IG_J}, \overline{S_IS_J}$	directed flux area	m^2
$\overline{G_iG_j}, \overline{G_iS_j}, \overline{S_iG_j}, \overline{S_iS_j}$	total exchange areas	m^2
h	convection heat transfer coefficient	$W\ m^{-2}\ K^{-1}$
H	specific enthalpy	$MJ\ kg^{-1}$
k	thermal conductivity	$W\ m^{-1}\ K^{-1}$
$k_{g,n}$	grey gas absorption coefficient	$m^{-1}\ atm^{-1}$
K_d	derivative gain	-
K_i	integral gain	-
K_p	proportional gain	-
LHV	Low heating value of fuel	$MJ\ kg^{-1}$
$\dot{m}_i$	mass flow rate of gas zone i	$kg\ s^{-1}$
$\dot{m}_{in}$	input mass flow rate	$kg\ s^{-1}$
$\dot{m}_{out}$	output mass flow rate	$kg\ s^{-1}$
M_b	Fuel and air mass input from burners	$kg\ s^{-1}$
M_e	Flue gas mass output from exhaust	$kg\ s^{-1}$
P_b	proportional band	$°C$
Q_a	preheated air energy input	MW
Q_b	energy transferred to steel blooms	MW
Q_{wc}	energy transferred to the furnace water cooling	MW
Q_e	energy in exhaust gases as they leave the furnace	MW
Q_f	fuel energy input	MW
Q_l	energy losses to furnace walls	MW
$\dot{Q}_a$	heat release from air	MW
$\dot{Q}_{conv}$	heat convection term	MW
$\dot{Q}_{fuel,net}$	heat input of fuel	MW
$\dot{Q}_{enth}$	enthalpy transport term	MW
$\dot{Q}_{wc}$	heat losses through the water-cooling	MW
$\dot{q}_{conv}$	heat flux to a surface zone by convection	$MW\ m^{-2}$
R	R-squared value	-
SFC	specific fuel consumption	$GJ\ tonne^{-1}$
SF	shadowing factor	-
t	elapsed time	s
T	temperature	$°C$
T_a	ambient temperature	$°C$
T_g	temperature of gas zone	$°C$
T_s	temperature of surface zone	
T_{sp}	set-point temperature	$°C$
dt	time-step	s
u	output of PID controller	$°C$
v	normalized output	-
V_i	volume of gas zone i	m^3
$X_{i,\ j\ or\ k}$	independent variables	-
y	predicted temperature	$°C$
Y	predicted inter-zone volumetric flow rate	$kg\ s^{-1}$
Z	reduced temperature	-
α	thermal diffusivity	$m^2\ s^{-1}$
β_0	model constant	-
β_i	linear coefficient	-
β_{ij}	quadratic coefficient	-
β_{ijk}	cubic coefficient	-
ρ	density	$kg\ m^{-3}$
σ	Stefan-Boltzmann constant (5.6687×10^{-8})	$W\ m^{-2}\ K^{-4}$
ϕ	property of materials	-
τ	time integral variable	s

1. Introduction

Large continuous walking-beam reheating furnaces are used extensively in the modern steel industry to heat intermediate steel products such as blooms, billets or slabs (known as stock) to a specific temperature and through-thickness temperature uniformity prior to hot-rolling. Therefore most reheating processes require precise control of the stock temperature over the entire heating period. One major difficulty however, is that the stock temperature is typically not available as continuously measured data, and is accessible only by periodic instrumented trials. Over the years, considerable efforts [1-2] have been made to circumvent this difficulty, resulting in the incorporation of online heating models in modern reheating furnace control systems to predict the stock temperature as it moves through the furnace. The online process controllers rely on these heating models to calculate and infer suitable zone temperature set points to dedicated plant controllers such that the stock is heated to its required discharge temperature, with an acceptable temperature level and distribution across and through the stock.

Considerable research effort in improving online heating models has been demonstrated recently, particularly in regard to more rigorous treatment of radiation exchange within the furnace enclosure [3-5]. Despite the improvements made, existing models still rely largely on empirical estimation of effective radiation-source temperature profiles along the furnace, usually through interpolation from a relatively limited set of thermocouple measurements, to determine the net rate of radiation heat transfer to the stock surfaces. Furthermore, these models do not take into account the full energy balances within the furnace and hence their application for more rigorous process optimisation is limited, particularly when competing factors from heated product quality and furnace efficiency are to be assessed simultaneously. Consequently, emphasis is given in the current paper to the development of more comprehensive mathematical models which can be used as offline (but still relatively fast) tools by furnace operators to investigate more generic aspects of furnace operation and control.

Although Computational Fluid Dynamics (CFD) techniques have been the most widely used methods to simulate combustion systems [6-9] with detailed local information (species concentration, temperature, velocity field etc.), they often take several days if not weeks to provide useful results for large industrial cases. Therefore, CFD techniques are entirely unsuitable for studying the transient behaviour of a practical reheating furnace in real or near real-time. An alternative approach is to use mathematical models based on the zone method of radiation analysis [10], namely 'zone models', in which the furnace enclosure is split into a finite number of gas and surface zones. In these models, the other mechanisms of heat transfer (convection and conduction) are incorporated in the radiation analysis. Solutions for the estimation of energy balance are then produced, taking into account all enthalpy transport and source terms associated with the flow of combustion products and their heat release due to combustion. Mathematical models based on the zone method have modest computational requirements and have been found to provide accurate representation of thermal performance for a wide range of industrial furnaces and boilers [11-14].

However, a particular challenge associated with the zone model is that it does not calculate the furnace flow pattern, and thus this information must be determined by some other means. Traditionally, plug flow or prediction from confined jet theory [15] have been adopted, but these are only reasonably valid for relatively long tunnel-shaped furnaces or for furnaces with simple uni-directional burner arrangements. Consequently these assumptions are not valid for modern reheating furnaces equipped with more complex burner arrangements in which the overall flow pattern within the furnace is highly three-dimensional.

Previous work at the University of South Wales [16] has been directed at demonstrating that sufficiently accurate furnace flow patterns can be obtained by 'one-off' isothermal CFD simulations through adopting the Thring-Newby scaling criterion [17]. This particular technique works well if only individual steady-state furnace operating conditions are to be simulated. However, when performing transient simulation, flow fields corresponding to each time-step in the transient zone model are required, but these cannot normally be pre-determined since they are a function of the burner inputs which in turn are modulated by the temperature controller during the simulation.

In view of the above, a suitably fast interpolation scheme has been developed which utilises a quadratic model to fit a representative set of isothermal CFD flow fields sampled by Box–Behnken designs [18]. Previously, this approach has been adopted in a two-dimensional transient zone model and results were validated by experiments performed on a pilot-scale walking beam furnace [19]. This paper describes the development of this approach into a three-dimensional transient zone model of a large-scale production furnace. The developed model is validated with plant measurements from a trial in which a sufficiently severe transient condition, due to a delay in production, was encountered.

2. Furnace zoning arrangement and operating conditions

The furnace studied has an effective length of 36 m and width of 10 m (illustrated in Figure 1). The furnace height varies between 4.0 m and 4.7 m along the length of the furnace. In total 71 burners are installed within 6 control zones which fire low-heating-value (*LHV*: 8.73 MJkg^{-1}) mixed enhanced fuel gas with a typical stoichiometric air requirement of 2.21 kg air/kg fuel.
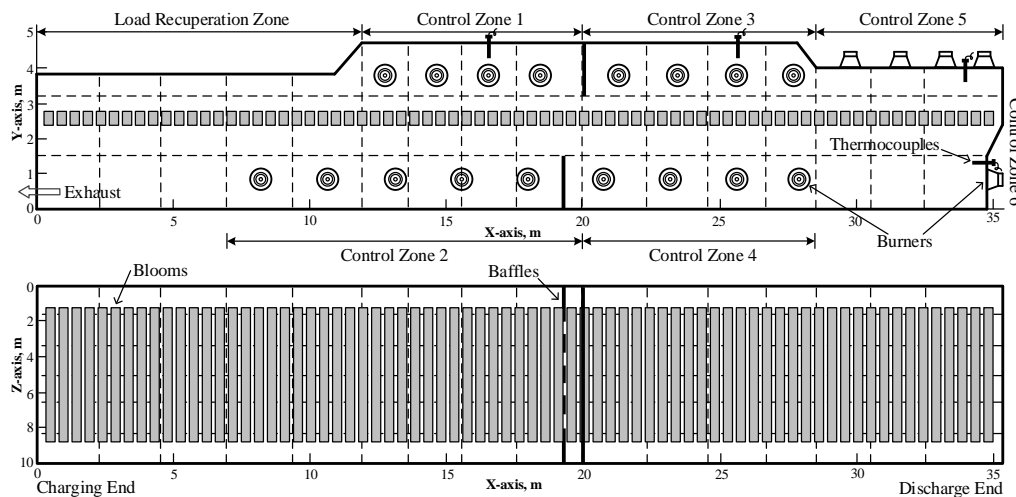

Figure 1. Outline of the furnace and zoning arrangement in *XY*- (upper) and *XZ*- (lower) plane

Zones 2 and 4 are slaves to control zones 1 and 3 respectively, in other words, their thermal inputs are set implicitly in proportion to the thermal inputs of the master control zones. The excess air used in control zone 5 was 0.5 and that in all other control zones was 0.8. The baffle walls physically isolate the neighbouring control zones from direct flame radiation interaction. The hot combustion gases leaving the furnace (via two exhaust ducts at the bottom of the load recuperation zone) pass through a radiant recuperator in which incoming combustion air is preheated to a temperature of approximately 419°C. In accordance with the zone method, the furnace was split into 16 sections (across its length) × 3 sections (across its height) × 6 sections (across its width); in total there are 288 volume zones and 794 surface zones (including 324 surface zones for furnace walls, 32 surface zones for baffle walls, and 438 surface zones for bloom surfaces).

Previously, Tata Steel had conducted an instrumented bloom trial to investigate the actual stock heating profile. During this trial period, the furnace was operating at a production rate of 127 tonnes per hour, where a total of 73 blooms of dimension 0.355m×0.305m×7.5m were linearly arranged and transported via a water-cooled walking-beam mechanism. As a result, a bloom was discharged approximately every 180 s. At 150 mins into operation, a delay in production was encountered which lasted for approximately 120 mins before production resumed again at 270 mins. In total, 466 tonnes of steel were heated to an average mean bulk temperature of 1250 °C during the 341 mins of furnace operation.

3. Model development

According to the zone method of radiation analysis, an energy balance is formulated for each zone (as shown in Figure 2) taking into account radiation interchange between all surface and volume zones, the enthalpy transport, source terms associated with the flow of combustion products and their heat release due to combustion [20].
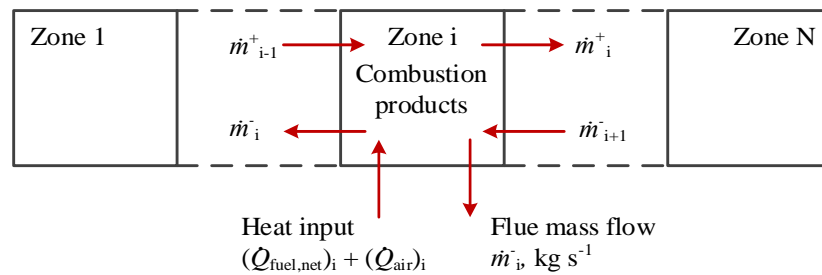

Figure 2. Flow field specifications for the zone model [20]

The radiation component in the energy balance equations is written in terms of exchange factors known as directed flux areas (denoted by $\overleftarrow{G_i G_j}, \overleftarrow{G_i S_j}, \overleftarrow{S_i G_j}, \overleftarrow{S_i S_j}$ for gas-gas, gas-surface, surface-gas, and surface-surface exchange respectively in Eq. 1 and 2), which allow for the effects of surface emissivity and the non-grey behaviour of the radiant interchange within the furnace enclosure. The energy balances on all zones yield a set of simultaneous non-linear equations which can be solved to determine the temperature and heat flux at each zone. The time-dependent internal node temperatures of blooms and wall lining can also be calculated by incorporating a transient conduction model.

For a system of N volume zones and M surface zones, the following energy balances can be written.

For the i-th volume (gas) zone:

$$\sum_{j=1}^{N} \overline{G_i G_j} \sigma T_{g,j}^4 + \sum_{j=1}^{M} (1 - A_d/A_j) \overline{G_i S_j} \sigma T_{s,j}^4 - 4 \sum_{n=1}^{n_g} a_{g,n} k_{g,n} V_i \sigma T_{g,i}^4 - (\dot{Q}_{conv})_i \qquad \text{(Eq. 1)}$$
$$+ (\dot{Q}_{fuel,net})_i + (\dot{Q}_a)_i + (\dot{Q}_{enth})_i - (\dot{Q}_{wc})_i = 0.$$

Likewise, for the i-th surface zone:

$$\sum_{j=1}^{M} (1 - A_d/A_j) \overline{S_i S_j} \sigma T_j^4 + \sum_{j=1}^{N} \overline{S_i G_j} \sigma T_{g,j}^4 - A_i \varepsilon_i \sigma T_i^4 + A_i (\dot{q}_{conv})_i = \dot{Q}_i \qquad \text{(Eq. 2)}$$

Radiation loss through the discharge door is modelled by assuming that the door occupies a fixed fraction (A_d/A_j) of a specified surface zone j of surface area A_j and 'shares' its exchange areas. The presence of a door does not affect the quantity of radiation arriving on it from all other zones in the enclosure, but it does however reduce the radiation that is both reflected and re-emitted from this surface zone. The emitted radiation is assumed to be reduced by a factor ($1-A_d/A_j$) in Eq. 1 and Eq. 2 when the door is open, which lasts for approximately 50 seconds while a bloom is being discharged. This treatment of the door loss is similar in concept to the speckled enclosure model of *Hottel and Sarofim* [10]. Moreover, in Eq. 1 the determination of heat losses through the water-cooled skid and upright structure ($\dot{Q}_{wc}$) follows that of Newton's law of cooling by specifying an appropriate overall heat transfer coefficient (which accounts for the effects of thermal resistance due to conduction, convection and radiation) from the gas to water side and the respective exposed surface areas in each gas zone. Energy flow considered in the model is shown in the Sankey diagram (Figures 3).

Q_f, fuel energy input.
Q_a, preheated air energy input
Q_b, energy transferred to steel blooms.
Q_e, energy in exhaust gases as they leave the furnace.
Q_{wc}, energy transferred to the furnace water cooling.
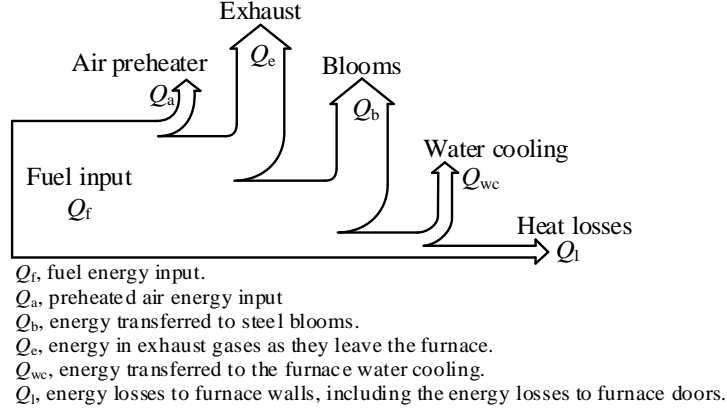Q_l, energy losses to furnace walls, including the energy losses to furnace doors.

Figure 3. Sankey diagram of the furnace model

Figure 4 shows the overall flow chart of the transient zone model. First from a given initial boundary condition the volume-zone energy balance equations (Eq. 1) are solved using the Newton-Raphson method [21], to yield the gas-zone temperatures (T_g). The calculated gas-zone temperatures are then substituted into the surface-zone energy balance equations (Eq. 2) to determine the rate of heat transfer to each surface zone corresponding to the blooms and furnace wall lining. The temperature distributions within the blooms and wall lining can then be updated by means of a finite difference conduction analysis. The effect of continuous

transport of blooms on their temperature-distance history along the furnace was simulated by a series of discrete pushes at fixed time intervals. At each push, one bloom is discharged, and the positions of all remaining blooms (together with their nodal temperatures) within the furnace are shifted forward towards the discharge end. The first bloom position at the charge end is then substituted with a new bloom at ambient temperature. Operating conditions can also be changed at a specific point in time if necessary, such as production rate and burner fuel flow rates. At the end of each time-step the quadratic flow model (described in Section 3.2) re-calculates the flow field inferred by new burner fuel flow rates which are modulated by the temperature controller. It should be noted that transient response of the flow field between consecutive time-steps is neglected and the quadratic interpolation scheme simply interpolates the flow field from one steady state to another. This assumption is reasonable as the time-step used in the transient zone model is relatively small compared to the time-constant of the furnace thermal response. The whole procedure can then be repeated sequentially over a series of time steps to predict the transient furnace operation. The following sub-sections describe each module in the flowchart in more detail.
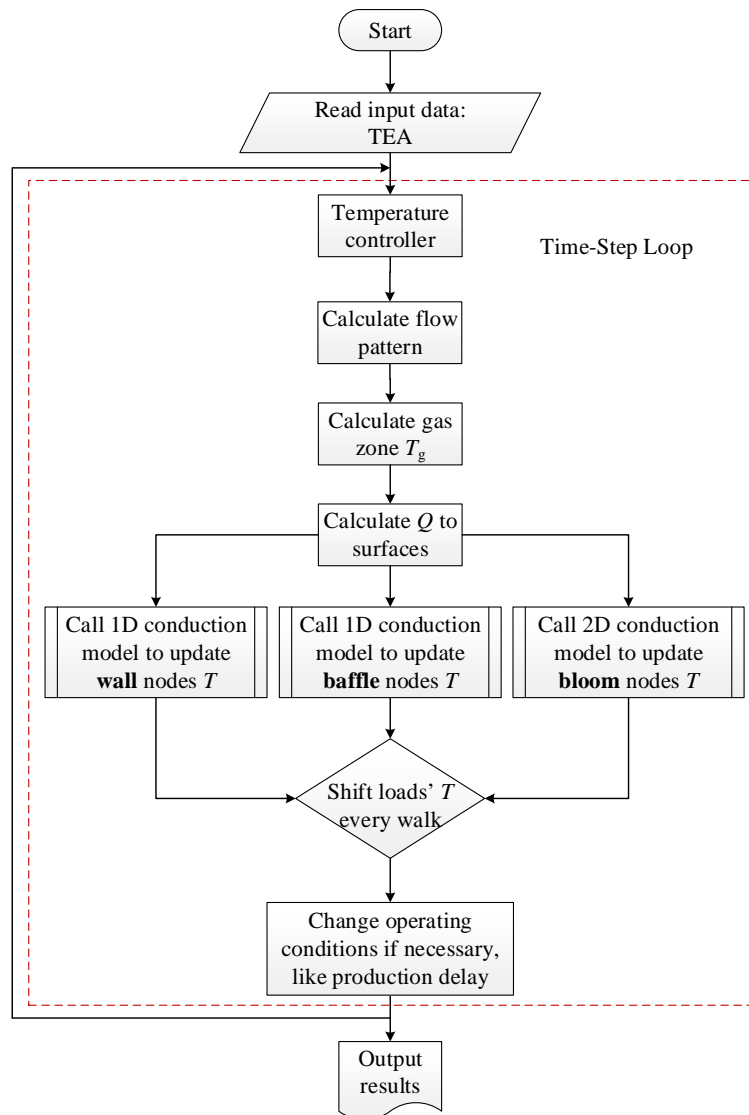

Figure 4. Program flow-chart of the transient zone model

3.1. Calculation of radiation exchange factors

The directed flux areas defined in Eq. 1 and Eq. 2 represent the radiant flux between each zone-pair and are expressed as the *a*-weighted summation of the total exchange areas (TEAs) for each of the number of grey gases used to approximate the radiative behaviour of real gases (known as Weighted Sum of mixed Grey Gases (WSGG) model [20]), defined as follows:

Gas – Surface directed flux area,

$$\overleftarrow{G_i S_j} = \sum_{n=1}^{N_g} a_{g,n}\left(T_{s,j}\right)\left(\overline{G_i S_j}\right)_{k=k_{g,n}},$$ (Eq. 3)

Surface – Surface directed flux area,

$$\overleftarrow{S_i S_j} = \sum_{n=1}^{N_g} a_{s,n}\left(T_{s,j}\right)\left(\overline{S_i S_j}\right)_{k=k_{g,n}},$$ (Eq. 4)

Gas – Gas directed flux area,

$$\overleftarrow{G_i G_j} = \sum_{n=1}^{N_g} a_{g,n}\left(T_{g,j}\right)\left(\overline{G_i G_j}\right)_{k=k_{g,n}}.$$ (Eq. 5)

The TEAs (denoted by $\overline{G_i S_j}$, $\overline{S_i S_j}$ and $\overline{G_i G_j}$) are calculated using an updated Monte-Carlo based Ray-Tracing (MCRT) algorithm [22] which takes into account individual stock geometry. It should be noted that the physical structures of the walking-beam and uprights were not directly taken into consideration during ray tracing (due to unnecessary complexity), and instead their effects of radiation shadowing to the bottom surface of the blooms were approximated by correcting the corresponding rate of surface radiant heat transfer by a constant shadowing factor (*SF* = 0.9). As mentioned in Section 2, the furnace uses mixed enhanced gas as fuel which is considerably different from natural gas in regard to its combustion product compositions. Hence a new set of WSGG model parameters for this mixed enhanced fuel gas, as reported in *Tan et al.* [16], has been adopted.

In this case the weighting coefficients ($a_{g,n}$ and $a_{s,n}$) in the above equations have been described by second-order polynomials in both T_g and T_s as follows:

$$a_{g,n}\left(T_g\right) = b_{1,n} + b_{2,n}T_g + b_{3,n}T_g^2$$ (Eq. 6)

and

$$a_{s,n}\left(T_s\right) = b_{1,n} + b_{2,n}T_s + b_{3,n}T_s^2.$$ (Eq. 7)

3.2. Furnace flow pattern

The volume-zone energy balance equations described earlier require knowledge of the enthalpy transport term ($\dot{Q}_{enth}$) due to the flow of hot combustion gases within the furnace. This in turn requires knowledge of the inter-zone mass flow rate within the furnace. In other words for each inter-zone boundary plane, it is necessary to calculate the mass flow into and out of the zone, illustrated in Figure 5, which presents an example single longitudinal sectional-view of the furnace corresponding to typical operating condition. It is evident that substantial flow recirculation may occur and the flow pattern is obviously far from being plug flow.
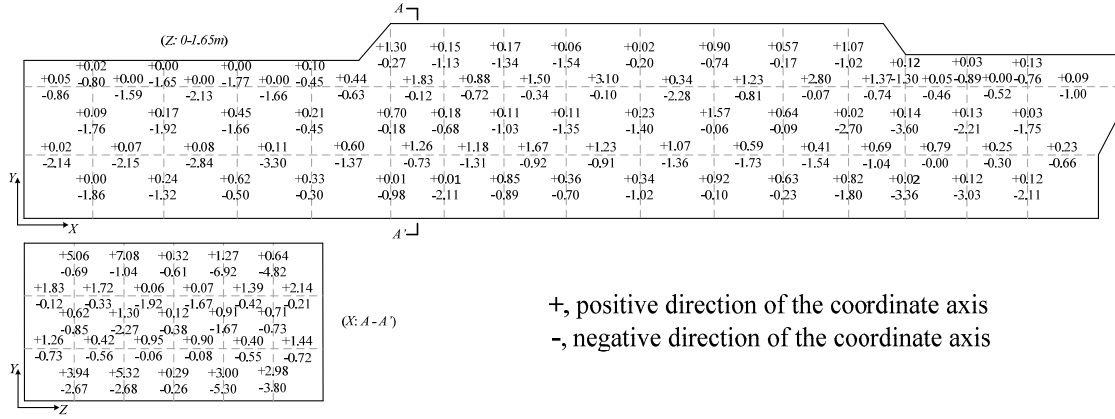
(Z: 0-1.65m)

```
                                                              A┐
                                               +1.30  +0.15  +0.17  +0.06   +0.02   +0.90   +0.57   +1.07
                                               -0.27  -1.13  -1.34  -1.54   -0.20   -0.74   -0.17   -1.02  +0.12  +0.03  +0.13
     +0.02   +0.00   +0.00   +0.10
+0.05 -0.80 +0.00 -1.65 +0.00 -1.77 +0.00 -0.45 +0.44 +1.83  +0.88  +1.50   +3.10   +0.34   +1.23   +2.80  +1.37-1.30 +0.05-0.89 +0.00-0.76  +0.09
     -0.86   -1.59   -2.13   -1.66  -0.63  -0.12  -0.72  -0.34   -0.10   -2.28   -0.81   -0.07   -0.74   -0.46   -0.52   -1.00
     +0.09   +0.17   +0.45   +0.21        +0.70  +0.18  +0.11  +0.11   +0.23   +1.57   +0.64   +0.02   +0.14   +0.13   +0.03
     -1.76   -1.92   -1.66   -0.45        -0.18  -0.68  -1.03  -1.35   -1.40   -0.06   -0.09   -2.70   -3.60   -2.21   -1.75
+0.02  +0.07   +0.08   +0.11        +0.60  +1.26  +1.18  +1.67  +1.23   +1.07   +0.59   +0.41   +0.69   +0.79   +0.25   +0.23
-2.14  -2.15   -2.84   -3.30        -1.37  -0.73  -1.31  -0.92  -0.91   -1.36   -1.73   -1.54   -1.04   -0.00   -0.30   -0.66
     +0.00   +0.24   +0.62   +0.33        +0.01  +0.01  +0.85  +0.36   +0.34   +0.92   +0.63   +0.82   +0.02   +0.12   +0.12
     -1.86   -1.32   -0.50   -0.30        -0.98  -2.11  -0.89  -0.70   -1.02   -0.10   -0.23   -1.80   -3.36   -3.03   -2.11
                                                              A'┘
```

```
 +5.06  +7.08  +0.32  +1.27  +0.64
 -0.69  -1.04  -0.61  -6.92  -4.82
+1.83 +1.72 +0.06 +0.07 +1.39 +2.14
-0.12 -0.33 -1.92 -1.67 -0.73 -0.21
    +0.62   +1.30   +0.12   +0.91   +0.42   +0.71
 -0.85  -2.27  -0.38  -1.67  -0.73
+1.26 +0.42 +0.95 +0.90 +0.40 +1.44
-0.73 -0.56 -0.06 -0.08 -0.55 -0.72
 +3.94  +5.32  +0.29  +3.00  +2.98
 -2.67  -2.68  -0.26  -5.30  -3.80
```

(X: A - A')

+, positive direction of the coordinate axis
-, negative direction of the coordinate axis

Figure 5. Illustrative single longitudinal sectional-view of inter-zone mass flow rate (kg s^{-1})

Similarly to the approach used in the previous pilot-scale study [19], Box-Behnken designs were used to determine the range of experimental points for conducting the isothermal CFD simulations. In the current case, the experimental designs consist of 4 factors, representing one group of burners in each of the four furnace control zones (i.e. control zones 1, 3, 5 and 6). The thermal capacity of each group of burners was divided into 5 levels, namely 0%, 25%, 50%, 75% and 100%, which resulted in 125 experimental points. The inter-zone volumetric flow rates (dependent variables) were thus correlated to the burner velocities (independent variables) via a series of quadratic models in the form of Eq. 8.

$$Y = \beta_0 + \sum_{i=1}^{4}\sum_{j=1}^{4}\sum_{k=1}^{4}(\beta_{ijk}X_iX_jX_k + \beta_{ij}X_iX_j + \beta_iX_i), \qquad (k \geq j \geq i) \tag{Eq. 8}$$

where: Y is the predicted inter-zone volumetric flow rate (kg s^{-1}); β_0 is a model constant; X_i, X_j and X_k are independent variables representing the burner velocities; β_i are linear coefficients; β_{ij} and β_{ijk} are cross product coefficients (or quadratic and cubic coefficients when i = j and i = j = k respectively).

The divisions of the zone model resulted in 708 internal planes being generated from which flow data were required. To predict the flows sufficiently accurately it was necessary to have a highly orthogonal computational mesh and hence a pure hexahedral mesh was created with a nominal cell length of 50mm giving a mesh size of approximately 30 million cells. A series of isothermal CFD simulations that defines the experimental points derived from the Box-Behnken designs were carried out using open-source CFD software OpenFOAM® [23]. It should be noted that the furnace was equipped with nozzle mix burners [24] and hence complete combustion may be assumed within the burners so that 100% heat is released into the immediate furnace volume zone where the burners are attached. In such a situation the combustion and hence the heat release profile within the furnace need not be considered. Consequently flows issuing from the burners are simply the products of complete combustion. Furthermore, the Thring-Newby scaling criterion [17] was employed to conserve the ratio of momentum flow rates of the combustion products from burners to that within the furnace under isothermal condition. The only model needed to be activated in the isothermal CFD was

a standard k-ε turbulent model which is considered adequate in representing turbulent flow encountered in a wide range of industrial furnaces. Consequently the run time of an isothermal CFD is considerably shorter than that of a full CFD simulation which takes into account also combustion and heat transfer. Hence, several hundreds of cases could be efficiently managed by a relatively small cluster of distributed computing facility.

In order to validate the above approach, 25 additional unseen CFD cases (i.e. not included in the initial experimental design) were compared to the values predicted by Eq. 8, as illustrated in Figure 6 for a small selection of the test cases. The results indicated that the fitted quadratic model provides reasonable approximation (R^2 value of 0.9811) to the actual CFD model.
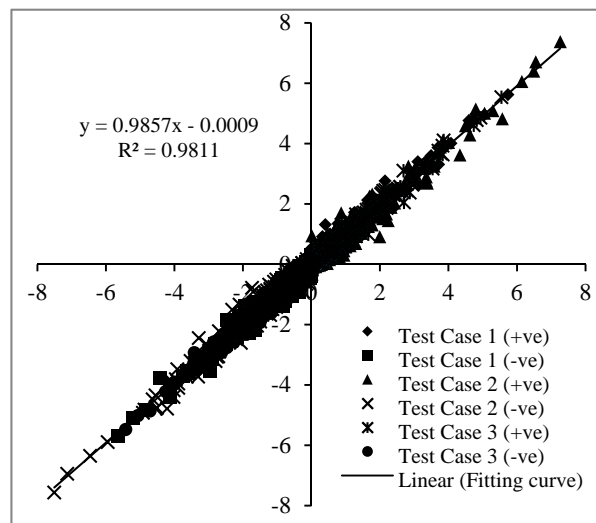
Figure 6. Comparison of the CFD (horizontal) and function calculated (vertical) volume flow rates (kg s^{-1}) for three test cases not in the initial experimental design
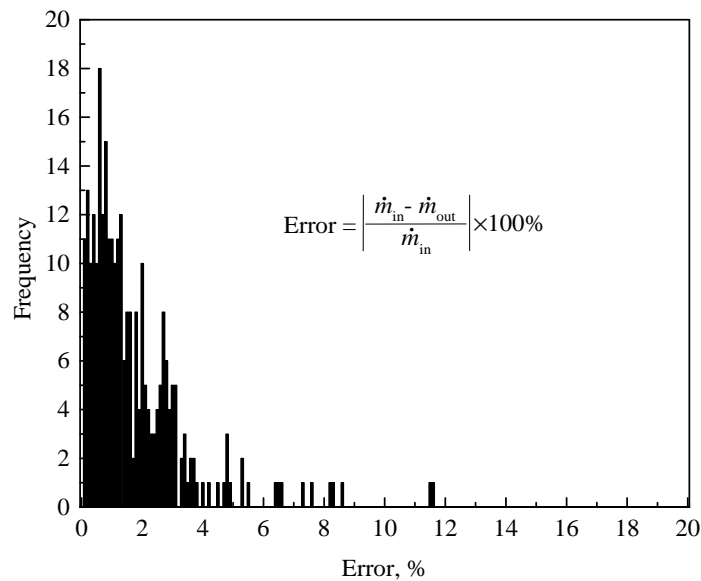
Figure 7. Error histogram of mass imbalance in each zone

Figure 7 further illustrates typical mass imbalance for each volume zone, expressed as percentage error relative to the total mass flow into that zone. The error histogram shows that the average mass imbalance in each volume zone was less than 1.8%. About 60% of the total 288 volume zones accounted for mass imbalances of less than 2%. It is worth noting that larger errors (above 5%) were only encountered in volume zones with relatively small mass flow rates and consequently this poses minimal impact on the accuracy of the overall global mass imbalance (less than 1%), i.e. the difference between the total mass flow into and out of the furnace.

The calculated isothermal flow field together with the temperature-dependent specific enthalpy for the air and stoichiometric combustion products can therefore be used to calculate the inter-zone enthalpy transport term ($\dot{Q}_{\text{enth}}$) in Eq. 1. The temperature-dependent specific enthalpy can be calculated from the following correlation of Eq. 9 [20]:

$$H(T) = a + bZ + cZ^2 + dZ^3 + eZ^4 + fZ^5 \tag{Eq. 9}$$

where $Z = (T - 1400)/200$ represents the normalised temperature and a, b, c etc. are the polynomial coefficients given in [20]. To account for the fuel lean combustion conditions, the specific enthalpy of the combustion at a given excess air ratio can be calculated from the mass fraction weighted summation of the specific enthalpies of the stoichiometric products and of the excess combustion air.

3.3. Modelling transient heat conduction
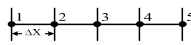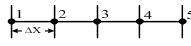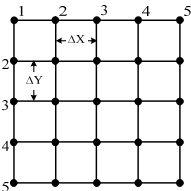
The transient zone model was described by applying the calculated surface heat transfer rates from the three-dimensional furnace enclosure (Eq. 2) as boundary conditions to the sets of one-dimensional (for walls and baffles) and two-dimensional (for blooms) Partial Differential heat conduction Equations (PDEs) as illustrated in Table 1. In the case of the outer furnace wall which is exposed to the ambient surroundings, combined convective and radiative boundary conditions were applied. These PDEs were then solved by the Crank-Nicolson finite-difference numerical method [25], which is relatively robust to the choice of time-step. For the two-dimensional transient conduction model, the alternating direction implicit solution procedure [26] was adopted to improve efficiency and stability while permitting a larger time-step to be used. For simplicity, the actual furnace wall structure was modelled as a single-layer dense refractory material and its average wall thickness is determined by matching the overall heat losses to those calculated from plant measurements.

The temperature-dependent material properties for the blooms (mild steel) and furnace refractory are described by the following polynomial equations:

$$\phi = a_1 + a_2 T + a_3 T^2 + a_4 T^3 + a_5 T^4 + a_6 T^5 + a_7 T^6 \,, \tag{Eq. 13}$$

where ϕ is the property (either k or C_{p}), T is the temperature in °C and a_i (i = 1,2,…,7) are polynomial coefficients [20].

Table 1. Boundary conditions and heat flow equations of different conduction models

	Dimensions	Boundary conditions	Heat flow equations	
Wall		$\dfrac{\partial T}{\partial n} = q,\ (\text{node 1});$ $\dfrac{\partial T}{\partial n} = -\dfrac{h}{k}(T - T_a)$ $-\dfrac{\varepsilon\sigma}{k}(T^4 - T_a^4),\ (\text{node 5}).$	$\dfrac{\partial^2 T}{\partial x^2} = \dfrac{1}{\alpha}\dfrac{\partial T}{\partial t},$	(Eq. 10)
Baffle		$\dfrac{\partial T}{\partial n} = q.$	$\dfrac{\partial^2 T}{\partial x^2} = \dfrac{1}{\alpha}\dfrac{\partial T}{\partial t},$	(Eq. 11)
Bloom		$\dfrac{\partial T}{\partial n} = q.$	$\dfrac{\partial^2 T}{\partial x^2} + \dfrac{\partial^2 T}{\partial y^2} = \dfrac{1}{\alpha}\dfrac{\partial T}{\partial t},$ $(\alpha = \dfrac{k}{\rho c_p}).$	(Eq. 12)

3.4. Implementation of furnace temperature controller

The simulation of the temperature control strategy is also considered in the transient zone model, since in practice the fuel flow rates are modulated in response to the measured thermocouple temperatures in each control zone. For this particular furnace, only 4 temperature controllers (for control zones 1, 3, 5 and 6) need to be simulated as the other two (control zone 2 and 4) are slaves (explained in Section 2). It is worth noting that, within the zone model, predicted temperatures from specific surface zones close to the actual thermocouple positions were used to simulate the controlled temperatures since in practice thermocouples are used to indicate wall temperature. A standard Proportional–Integral–Derivative (PID) controller [27] was implemented where the controller output $u(t)$ is calculated by summing the proportional, integral, and derivative terms such that:

$$u(t) = K_p e(t) + K_i \int_0^t e(t)dt + K_d \frac{d}{dt}e(t), \tag{Eq. 14}$$

where K_p, K_i and K_d denote the proportional, integral and derivative gains respectively, and $e(t)$ is the error, i.e. the difference between measured and set-point temperature in each control zone. In Eq. 14, $u(t)$ represents the required temperature compensation relative to the set-point temperature (T_{sp}) at the current time-step and this is then used to adjust the burner fuel flow rate (i.e. normalising the firing rate $v(t)$ between 0 and 1) in the beginning of the next time-step as defined in Eq. 15:

$$v(t + dt) = v(t) + \frac{F_{max} - F_{min}}{P_b}\left(T_{sp} - u(t)\right). \tag{Eq. 15}$$

The overall block diagram of the temperature controller is illustrated in Figure 8. Here F_{max} and F_{min} are respectively the normalized (between 0 and 1) maximum and minimum firing rates of the burners, as required by the format of fuel input to the zone model. In the current study, the controller parameters in Figure 8 have been tuned so that $K_p = 0.05$, $K_i = 0.5$, $K_d = 0.5$ and $P_b = 200$.
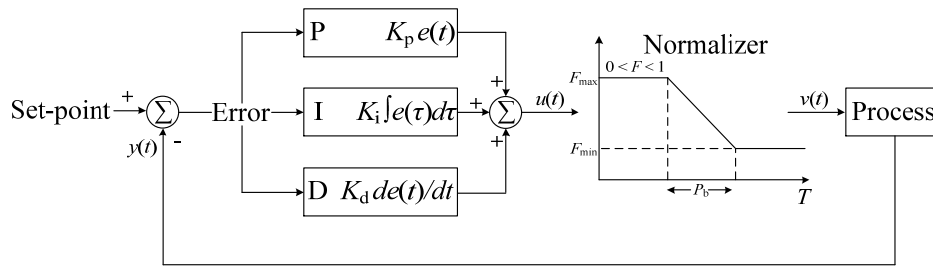
Figure 8. A block diagram of a normalized PID controller in a feedback loop

It should be noted that the time-delay associated with fuel and air valve operation along the fuel and air piping are not considered in the current context and hence the burner firing rates in each control zone respond instantaneously to changes in the respective set-point temperatures.

4. Validation of the virtual furnace model

Before validation of the trial data proceeds, it is necessary to establish an initial furnace boundary condition for the zone model. As actual measurements are limited, this step was accomplished by running the zone model first from cold start-up until the furnace reaches a steady production condition. This is subsequently followed by tracing the control-zone set-point temperatures over the entire period of the instrumented bloom trial.

4.1. Simulation from cold start-up

In order to establish a reasonable initial furnace boundary condition for the zone model, the set-point temperatures used to start up the furnace were determined from the initial condition of the trial. Figure 9 shows that the furnace wall linings took approximately 48 hours to heat up from cold. This steady-state condition reasonably reflects the actual furnace condition after a prolonged period of continuous operation. At this point, the furnace energy and mass balance were also inspected, as shown in Table 2.
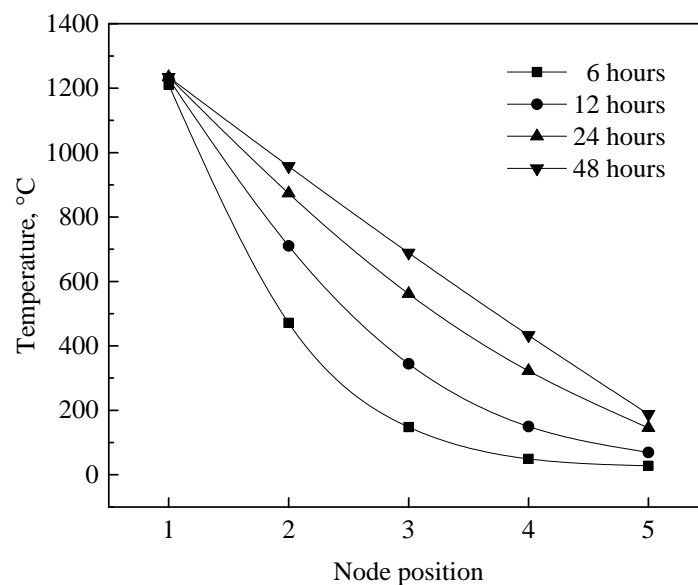

Figure 9 Evolution of furnace wall lining temperatures from cold start-up

Table 2 Energy and mass balance inspection at the steady state

	Source	Value	Imbalance
Energy input	Q_f	53.8 MW	
	Q_a	6.63 MW	
Energy output	Q_b	26.9 MW	0.3%
	Q_e	19.9 MW	
	Q_{wc}	8.09 MW	
	Q_l	5.00 MW	
Mass input	M_b	20.9 kg s^{-1}	<0.1%
Mass output	M_e	21.0 kg s^{-1}	

Q_f, fuel energy input.
Q_a, preheated air energy input
Q_b, energy transferred to steel blooms.
Q_e, energy in exhaust gases as they leave the furnace.
Q_{wc}, energy transferred to the furnace water cooling.
Q_l, energy losses to furnace walls, including the energy losses to furnace doors (0.67 MW).
M_b, fuel and air mass input from burners,
M_c, flue gas mass output from exhaust.

The energy input was broken down to fuel and air, and the energy output was broken down into the heat transfer to blooms (Q_b), walls (Q_l), water cooling (Q_{wc}), and heat loss in the exhaust (Q_e). The mass balance check was set up between the fuel and air mass input from burners and flue gas mass output from exhaust. This shows that the global energy and mass imbalances (difference between input and output) are 0.3% and less than 0.1% respectively.
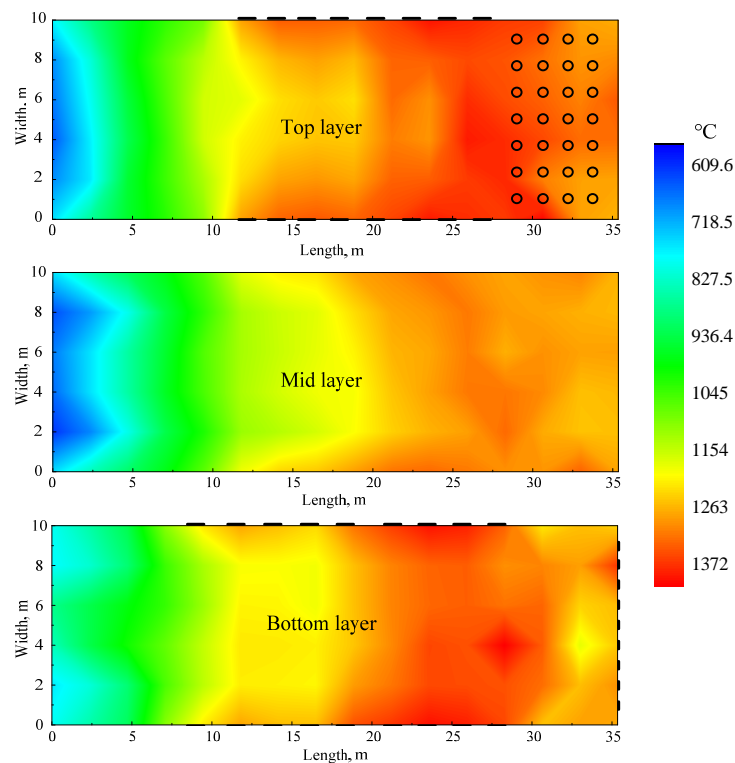
Figure 10 Gas temperature contour when the furnace reached the steady state

Figures 10 and 11 further illustrate the gas and wall temperature contours on the same colour scales. For clarity in discussion of the results, the burner positions are also overlaid. It can be

clearly observed that higher gas temperatures occur in regions in which burners are firing, in particular control zones 3 and 4. The gas temperature decreases when passing through the load recuperation region towards the charge end where the rate of heat transfer from the hot gases to the colder blooms increases. The gas zone temperature distribution also reflects the slightly non-symmetrical flow pattern generated by the swirled flat-flame burners installed on the roof of the soak zone. Further examination of Figure 11 also reveals no significant hot spots on furnace walls and the furnace wall temperature distribution follows that of the gas fairly consistently as expected.
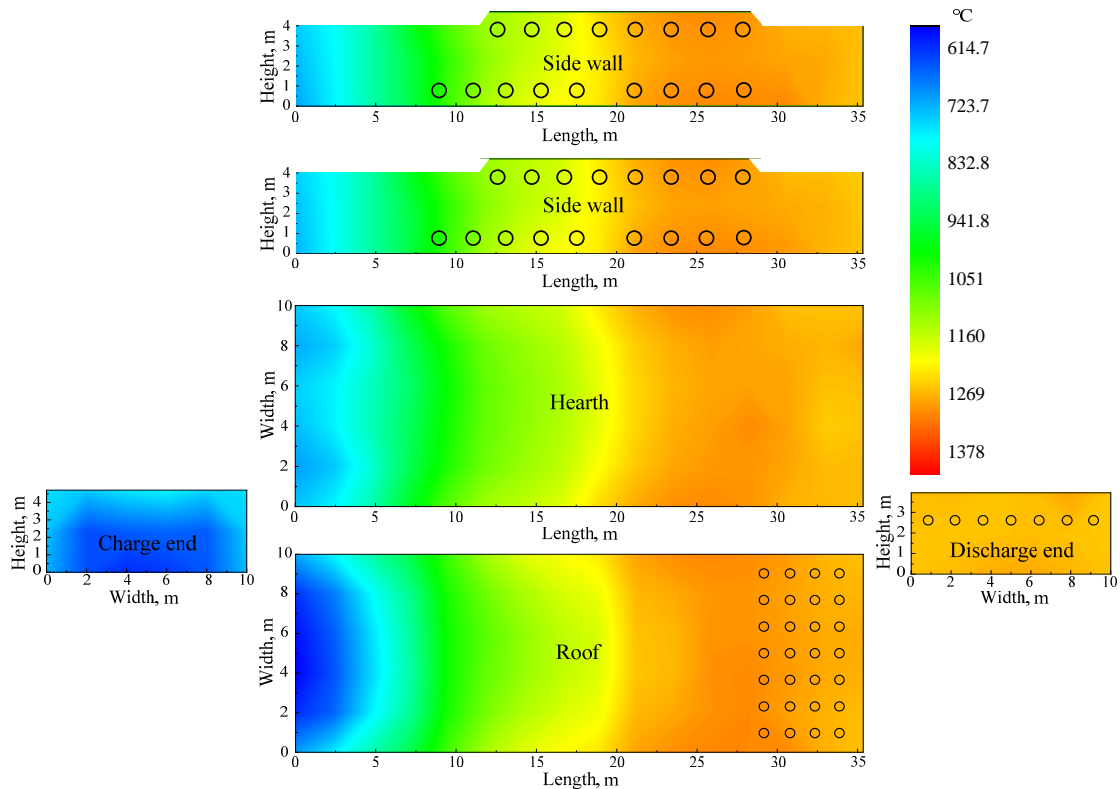
Figure 11 Wall temperature contour when the furnace reached the steady state
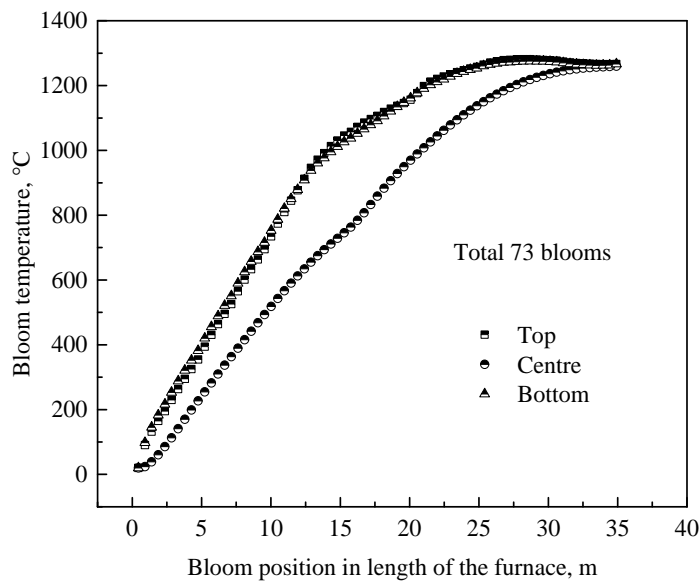
Figure 12 Top, centre, and bottom temperatures of the blooms at the steady state

In addition, Figure 12 shows the resultant heating profile of the blooms within the furnace with respect to current steady-state set-point temperatures and a production rate of 127 tonhr^{-1}. It can be observed that temperatures on the top and bottom surfaces of the blooms are comparable which implies consistency in the furnace set-point temperatures regulation by the PID controller. Under current steady production rate, the blooms are heated to a mean bulk temperature of 1250 °C with good temperature uniformity (maximum nodal temperature difference of less than 10 °C).

4.2. Comparison of model prediction with trial data

Based on the established initial conditions, simulation was performed for a further 341 mins during the period of instrumented bloom trial as described in Section 2. For the purpose of validating the dynamic response of the zone model, the time-varying set-point temperatures, as recorded during the trial, were input into the PID temperature controller, and subsequently, the specific wall temperatures (i.e. those simulating the measured temperature of the actual thermocouples) in each control zone and the temperature history of the blooms were predicted. Predictions from the zone model were also compared with those from the plant's level-2 model used within the exiting furnace temperature control system.

Figure 13 (a) shows the measured thermocouple temperature history in each control zone with respect to variation in the set-point temperatures during the trial, and the predicted thermocouple temperature is illustrated in Figure 13 (b). It can be seen that the trends for both the actual and predicted thermocouple temperatures (i.e. the controlled temperatures) were comparable although subtle differences are visible. Nevertheless, despite the assumptions made in the modelling and simulation, these results are encouraging. Both graphs also show consistent tracking of the furnace set-point temperatures, except in control zone 1 during the period of production delay, where the set-point temperature during the trial is believed to have been set intentionally to a relatively lower value in order to minimise heat input. Consequently, the measured thermocouple temperature was influenced purely by the flow of hotter combustion gases from neighbouring control zones upstream.
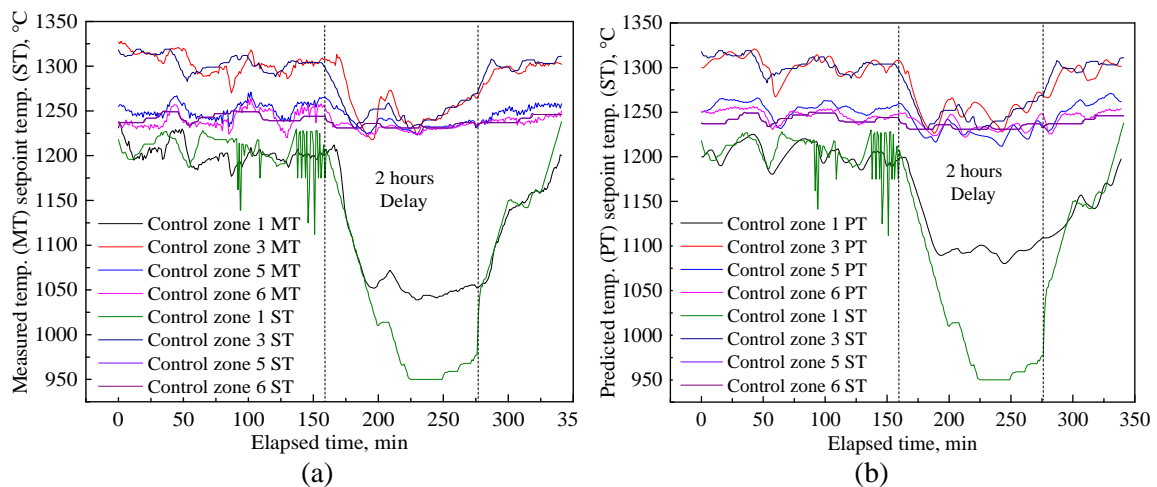

Figure 13 Comparisons of set-point temperatures, ST, with (a) actual thermocouple temperatures, MT and (b) predicted thermocouple temperatures, PT

The predicted top, centre, and bottom temperature histories also compared well, in general, with actual measurements as illustrated in Figure 14. Discrepancies between predicted and actual temperatures in the vicinity of the material phase-change region (approximately 750°C) are noticeable, particularly for the centre position. This may well be attributed to the approximated thermal properties of the material during the phase-change process. Nevertheless, it is clear that predictions from the zone model outperformed those of the existing level-2 model in most instances, which demonstrates the effectiveness of the modelling methodology.
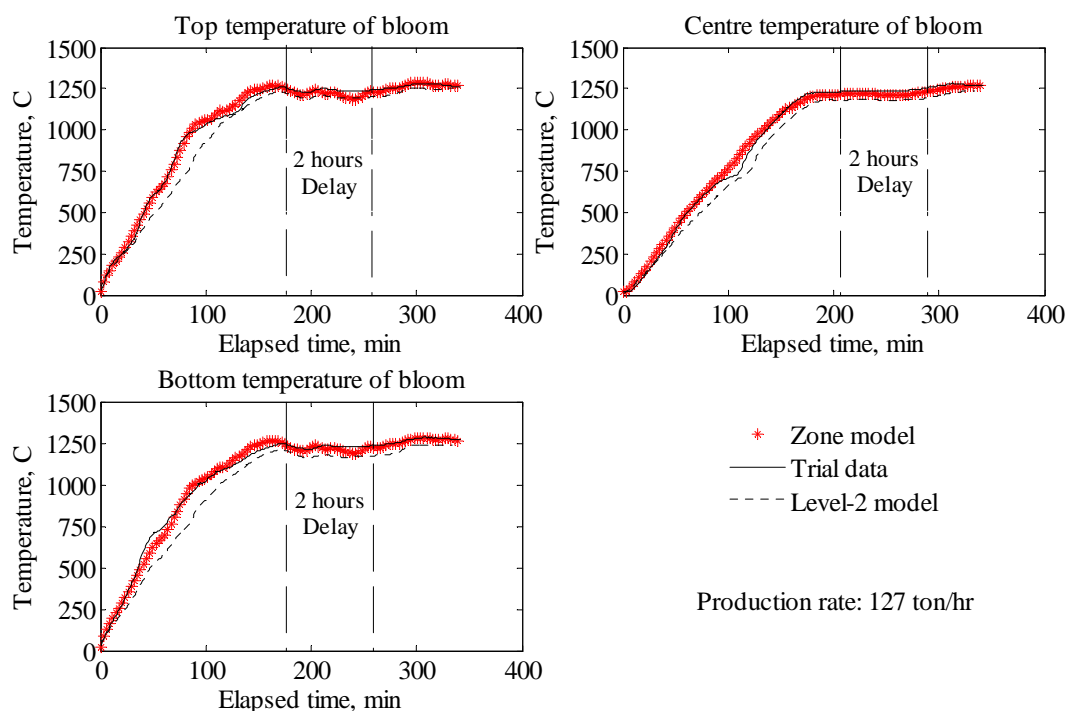

Figure 14 Predictions of the top, centre and bottom temperature histories of the instrumented bloom

4.3. Furnace energy balance audit

During simulation of the trial period, the cumulative thermal energy entering and leaving the furnace was also calculated as shown in Table 3 and this was compared with the benchmark energy balance derived from the same trial. First a benchmark simulation was conducted with time-step of 20s and the known water-cooled load adjusted to approximately 19% of the fuel thermal input. Subsequently with all model parameters fixed, simulations were repeated with two further time-steps of 5s and 45s. Examination of Table 3 suggests that the zone model was able to predict the overall thermal behaviour of the furnace with reasonable accuracy. From the perspectives of stability and convergence, the time-step only affects the transient conduction models but not the solution of flow field as discussed in Section 3. Although results from the investigated time-steps are comparable, the use of excessively large time-steps should be avoided due to potentially large numerical errors incurred by the finite difference scheme employed in the transient conduction model. Values should be chosen to adequately capture the dynamics of the furnace response.

Table 3. Comparison of furnace energy balance by trial data and zone model (ZM) results with different time-step setting

	Units	Energy input		Energy output				Performance		
		Q_f	Q_a	Q_b	Q_e	Q_{wc}	Q_l	E_c	E_f	SFC
Trial data	MW	41.6	5.5	18.9	15.9	8.1	4.2	75.1	45.5	1.76
	%Q_f	100.0	13.0	45.0	38.0	19.0	10.0			
ZM ($dt = 5$s)	MW	41.4	5.1	18.3	15.8	7.9	4.3	73.9	44.4	1.81
	%Q_f	100.0	12.2	44.4	38.3	19.0	10.4			
ZM ($dt = 20$s)	MW	41.1	5.0	18.2	15.7	7.9	4.2	74.0	44.4	1.79
	%Q_f	100.0	12.2	44.4	38.3	19.1	10.3			
ZM ($dt = 45$s)	MW	41.2	5.1	18.2	15.8	7.9	4.3	73.8	44.2	1.80
	%Q_f	100.0	12.3	44.2	38.4	19.1	10.5			

Q_f, fuel energy input.
Q_a, preheated air energy input
Q_b, energy transferred to steel blooms.
Q_e, energy in exhaust gases as they leave the furnace.
Q_{wc}, energy transferred to the furnace water cooling.
Q_l, energy losses to furnace walls, including the energy losses to furnace doors (0.67 MW).
E_c, combustion efficiency, $1+(Q_a/Q_f)-(Q_e/Q_f)$ as a percentage.
E_f, furnace efficiency, Q_b/Q_f as a percentage.
SFC, specific fuel consumption, Q_f/tonnes, usually expressed in GJ tonne^{-1}.

5. Product quality evaluation

The product quality was further evaluated using the validated virtual furnace model with respect to the mean bulk temperature and temperature uniformity of the drop-out bloom. During the production delay period the drop-out condition simply referred to condition of the last bloom prior to discharge. Since no plant data were available, results presented in Figure 15 are only those predicted by the zone model. Before the start of the production delay the drop-out mean bulk temperature was relatively stable to within ±10°C. However, this subsequently dropped by approximately 30°C at the end of the production delay period due to the lower set-point temperatures incurred on all control zones, before finally recovering to the level prior to the production delay.

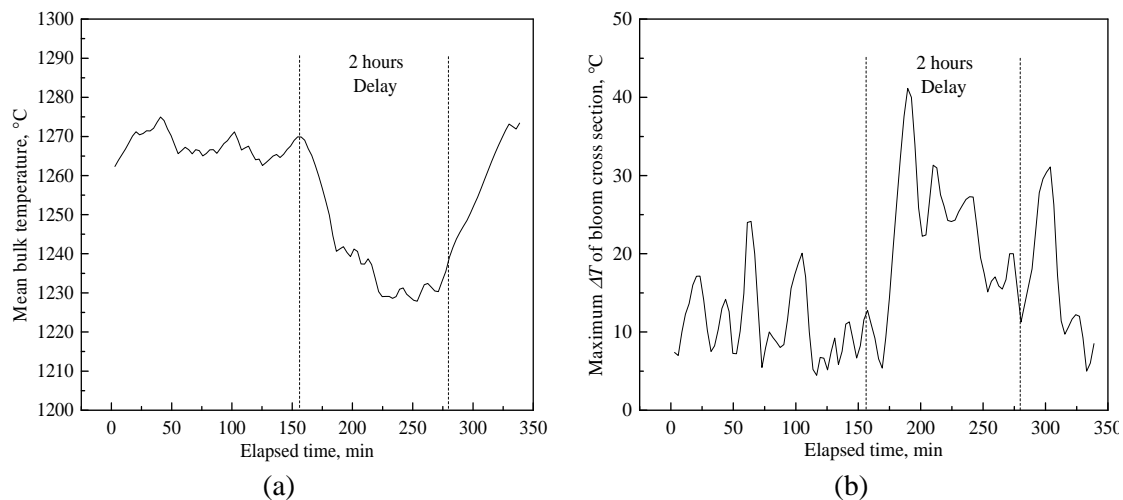(a)   (b)

Figure 15. Predicted mean bulk temperature (a) and temperature uniformity (b) history of the drop-out bloom during the simulated trial period

The results highlighted an important view that furnace set-point temperatures during delay should be optimised such that production may resume almost immediately without concern of under/over-heating and temperature uniformity if the duration of the delay is known. Consequently, the zone model enables detailed offline analysis of furnace operation to be performed such that improved understanding of the furnace temperature response can be gained and incorporated into furnace delay management strategies.

6. Model computational efficiency

As shown in Figure 16, even with consumer-level PC hardware, the computational efficiency of the zone model is fairly promising, given that there is additional scope for parallelizing the zone model program architecture, in particular the transient conduction module (see Figure 4). The results imply that the zone model is capable of real time simulation and has great potential to be used for parametric studies of furnace operating conditions or to be incorporated directly into dedicated furnace optimisation and control algorithms.
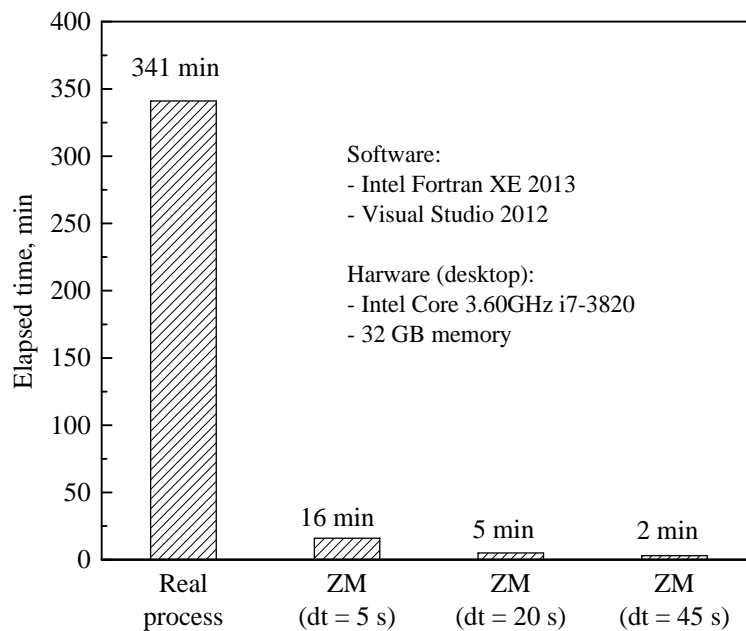

Figure 16. Comparison of the computing time of the cases with different time-step setting

6. Conclusions

This paper details the development of a first-principles hybrid model for large-scale reheating furnaces, and highlights a novel approach of integrating a real-time quadratic flow model into the classical zone method. By correlating a representative set of isothermal mass flow patterns for existing reheating furnace designed by the Box-Behnken method, the quadratic flow model is capable of predicting unseen mass flow patterns with reasonable accuracy. It has been demonstrated that the hybrid model executes 21 to 170 times faster than real-time (depending on the transient conduction time-step) and that it predicts the thermal performances of the furnace (such as overall furnace efficiency, specific fuel consumption and energy distribution) with good accuracy. Not only that, but the developed hybrid model also outperforms the semi-empirical level-2 model used in the existing plant when predicting

the heating profile of the instrumented bloom; the simulated controlled set-point temperatures of the model were able to correctly respond to the transient operating condition imposed by a typical period of production delay. Together with its relatively short computing time, the developed hybrid model could be well suited for incorporation into supervisory temperature control system or as an offline simulation tool for investigating furnace optimisation and control problems.

References
[1] Norberg PO. Challenges in the control of the reheating and annealing process. Scandinavian Journal of Metallurgy 1997; 26(5): 206-214.

[2] Staalman D. The funnel model for accurate slab temperature in reheating furnaces. Revue de Métallurgie 2004 ; 101(6): 453-459.

[3] Madsen EE. Steeltemp – A program for temperature analysis in steel plants. Journal of Materials Processing Technology 1994; 42(2):187-195.

[4] Yan W, Zhang F. Mathematical model study on billet heating furnace. Industrial Furnace 2000; 22(2): 54-58.

[5] Anton J, Tomaž K, Borut Z. The influence of the space between the billets on the productivity of a continuous walking-beam furnace. Applied Thermal Engineering 2005; 25(5-6): 783-795.

[6] Falcitellli M, Pasini S, Tognotti L. Modelling practical combustion systems and predicting NOx emissions with an integrated CFD based approach. Computers & Chemical Engineering 2002; 26(9): 1171-1183.

[7] Hu Y, Yan J. Numerical simulation of radiation intensity of oxy-coal combustion with flue gas recirculation. International Journal of Greenhouse Gas Control 2013; 17: 473-480.

[8] Hu Y, Li H, Yan J. Numerical investigation of heat transfer characteristics in utility boilers of oxy-coal combustion. Applied Energy 2014; 130: 543-551.

[9] Yin C, Yan J. Oxy-fuel combustion of pulverized fuels: Combustion fundamentals and modelling. Applied Energy 2016; 162: 742-762.

[10] Hottel HC, Sarofim AF. Radiative transfer. New York: McGraw-Hill Inc; 1967.

[11] Kouprianov VI. Modeling of thermal characteristics for a furnace of a 500 MW boiler fired with high-ash coal. Energy 2001; 26:839-853.

[12] Tucker R, Ward J. Identifying and quantifying energy savings on fired plant using low cost modelling techniques. Applied Energy, 2012; 89: 127-132.

[13] Correia SAC, Ward J. The application of a two-dimensional zone model to the design and control of a continuously operated, gas-fired furnace. Proceedings of the ASME International Mechanical Engineering Congress and Exposition, New Orleans, LA, United States; Nov 17-22, 2002; pp. 29-35.

[14] Tucker RJ, Ward J. Mathematical-modelling of heat-transfer in a gas-fired reheating furnace operating under non-steady state conditions. 9th International conf on Heat Transfer, Jerusalem, Israel; Aug 19-24. 1990; Vol.1-7, pp.221-226.

[15] Tucker RJ. Evaluation and development of the zone method for modelling metal heating furnaces. PhD Thesis, Faculty of Technology, Open University; 1990.

[16] Tan CK, Jenkins J, Ward J, Broughton J, Heeley A. Zone modelling of the thermal performance of a large-scale bloom reheating furnace. Applied Thermal Engineering 2013; 50: 1111-1118.

[17] Thring MW, Newby MP. Combustion length of enclosed turbulent jet flames. Fourth Symposium on Combustion, Williams and Wilkins, Baltimore; 1953; pp. 789-96.

[18] Ferreira LC, Bruns RE, Ferreira HS, Matos GD, David JM, Brandão GC, da Silva EGP, Portugal LA, dos Reis PS, Souza AS, dos Santos WNL. Box-Behnken design: An alternative for the optimization of analytical methods. Analytica Chimica Acta 2007; 597: 179-186.

[19] Hu Y, Niska J, Broughton J, McGee E, Tan CK, Matthew A, Roach PA. Zone modelling coupled with dynamic flow pattern for the prediction of transient performance of metal reheating. Proceeding of AISTech2014-The Iron & Steel Technology Conference and Exposition; Indianapolis, USA; May 5-8, 2014.

[20] Rhine JM, Tucker RJ, 1991. Modelling of gas-fired furnaces and boilers. New York: McGraw-Hill Inc; 1991.

[21] Hildebrand F. Introduction to Numerical Analysis. Dover Publications; 1987.

[22] Matthew AD, Tan CK, Roach PA, Ward J, Broughton J, Heeley A. Calculation of the radiative heat-exchange areas in a large-scale furnace with the use of the Monte Carlo method. Journal of Engineering Physics and Thermophysics 2014; 87(3): 732-742.

[23] OpenFOAM. <http://www.openfoam.com>.

[24] Jenkins B, Mullinger, P. Industrial and process furnaces: principles, design and operation. 2nd edition, Elsevier Ltd, UK; 2014.

[25] Crank J, Nicolson P. A practical method for numerical evaluation of solutions of partial differential equations of the heat conduction type. Proceedings of the Cambridge Philosophical Society 1947; 43 (1): 50–67.

[26] Croft DR, Lilley DG. Heat transfer calculations using finite difference equations. Applied Science Publishers Ltd, London; 1977.

[27] Astrom KJ, Hagglund T. PID controllers, theory, design and tuning. 2nd edition, Instrument Society of America; 1995.